Polymer Electrolyte Membranes Incorporated with Nanometer-Size Particles of Pt and/or Metal-Oxides: Experimental Analysis of the Self-Humidification and Suppression of Gas-Crossover in Fuel Cells

Masahiro Watanabe,* Hiroyuki Uchida, and Masaomi Emori

Laboratory of Electrochemical Energy Conversion, Faculty of Engineering, Yamanashi University, Takeda 4-3, Kofu 400, Japan

Received: October 28, 1997; In Final Form: February 10, 1998

Self-humidification behaviors of polymer electrolyte membranes (PEMs) were clarified experimentally in polymer electrolyte fuel cells (PEFCs) operated with dry H_2 and O_2. New PEMs (Pt−PEM, TiO_2−PEM, Pt−TiO_2−PEM) were prepared by dispersing small amounts of Pt (1−2 nm in diameter) and/or metal-oxides such as TiO_2 (5 nm in diameter) in Nafion 112 or a recasted Nafion film (normal-PEM, ca. 50 μm in thickness). Distribution profiles of the specific resistances (ρ) in thickness direction were measured with monitoring Pt-probes inserted into the PEMs. In normal-PEM, the ρ increases with increase of current density at the anode side and vice versa at the cathode side, and this was pronounced at high current density. However, it was found that the ρ decreased monotonically at every portion in Pt−PEM with increase of current density, although the ρ of anode side is larger than that of cathode side. Further uniform ρ distribution was achieved in Pt−TiO_2−PEM, i.e., $\leq$20 Ω cm at a practically operational current density. The mechanisms of such a distinctive self-humidification and a suppression of crossover of reactant gases in the new PEMs were clarified by monitoring consumed H_2 and O_2 and produced water in exhausting gases from PEFCs in comparison with normal-PEM. In Pt−TiO_2−PEMs, crossover H_2 and O_2 were recombined on Pt particles and all of the water generated inside the PEMs was exhausted from the anode. The TiO_2 particles enhanced the back-diffusion of water produced by faradic reaction at the cathode by the hygroscopic property, resulting in very efficient humidification of the PEM of the anode side dried by the electroosmotic drag. It was also found that the new PEMs improve the cathode potential distinctively, which was ascribed to elimination of the short-circuit reaction of crossover gases in the cathode catalyst layer, resulting in a small non-faradic consumption of H_2 and no disturbance of reactant O_2 diffusion by the produced water vapor.

Introduction

Polymer electrolyte fuel cells (PEFCs) are attracting enormous interest as a primary power source for electric vehicles or portable electric devices. Polymer electrolyte membranes (PEMs) such as Nafion used in these cells require water to maintain proton conductivity. The water content is changed in an extremely complicated manner with the operating conditions as shown by mathematical modeling and numerical calculation or by experiments.[1−21] In practical cells, so far, water content in PEMs has been managed indirectly by humidifying either the fuel gas or the fuel and oxygen. The reduction of PEM thickness reduces water management problems due to the water back-diffused from the cathode.[11] The reduction has a potential not only to reduce ohmic potential drop in the cell but also to improve the cathode performance.[22] However, this usually accelerates the crossover of H_2 and O_2 through the thin PEMs, which lowers the cell performance and the fuel utilization. Hence, the management of water content and of reactant crossover is recognized as a key technology for PEFCs.

Attempting to overcome these problems, we have proposed new PEMs highly dispersed nanometer-size Pt and/or metal-oxides.[23−25,30] The design concept for the Pt and metal-oxides dispersed PEM is schematically shown in Figure 1. The Pt particles were expected to inhibit the crossover by the catalytic recombination of crossover H_2 and O_2. On the other hand, the oxide particles that have hygroscopic property were expected to adsorb the water produced at Pt particles together with that produced at the cathode reaction and to release the water once the PEM needs water. The PEFCs with these new PEMs demonstrated the superior performances and suppression of the crossover even under externally nonhumidified condition, which are comparable to that of the conventional PEM fully humidified. Therefore, it is very important to clarify the self-humidifying mechanism from the viewpoint not only of the practical application but also of the basic science of PEMs.

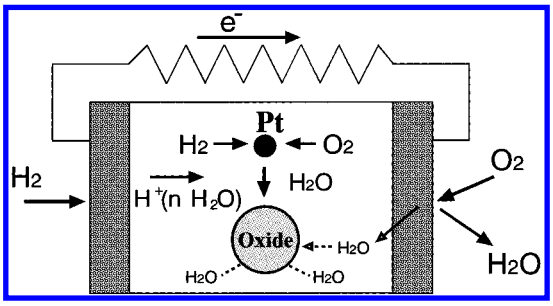

Figure 1. Schematic operation concept of a new PEFC using self-humidifying Pt−oxide−PEM.

Regarding the conventional PEMs, mainly Nafion 117 (ca. 170 μm in thickness), numerous studies have been performed

* American Chemical Society Active Member, to whom correspondence should be addressed. E-mail: mwatanab@ab11.yamanashi.ac.jp. Fax: 81-552-54-0371.

S1089-5647(97)03477-9 CCC: $15.00
Published on Web 04/02/1998

ex situ on parameters such as water uptake,[2,6−9] the nature of the water in PEMs,[16] water diffusion coefficients,[8,21] proton diffusion coefficients,[4] and ionic resistivity at different temperatures.[7,18] These results are very important for understanding the basic properties of proton conductance of the PEM. However, they do not provide enough insight into the dependence of the resistivity of these PEMs on the fuel cell operating conditions, because the resistivity in the operating cell may be influenced by many parameters such as current density, temperature, utilization of reactant gases (with respect to humidity), and cell design. So far, overall resistances of PEMs in the operating cells have been dealt with numerical estimation[11,12] or experiments,[17,19,25] and an increase of overall resistance of Nafion 117 with increasing current density has been demonstrated.[11,12,19] However, there are a few works regarding the distribution of specific resistance (ρ) or water in PEMs.[11,12,17] We have already clarified experimentally the distribution profiles of the ρ in a recasted conventional Nafion film operated under various humidity and current density,[17] which were performed by inserting fine probes for determination of the ohmic drops in different portions of the PEM. It was found that the ρ profiles are dramatically changed by the operation condition due to the electroosmotic drag and the back-diffusion of water from the cathode and show an extreme inhomogeneity in the thickness direction of the PEM even under the humidified conditions. Recently, another experimental approach using a neutron radiography was proposed for the monitoring of water transport profiles across Nafion in operating PEFCs,[21] but the validity is still unclear because of the low resolution. As clarified in the present work, the management of the ρ profiles reflecting water distribution rather than the overall resistance in PEMs is very important to design high-performance PEFCs.

From the background described above, it is essential to study more details on the behaviors of the humidification and crossover in PEMs, particularly in the self-humidifying new PEMs. In this paper, we clarify experimentally how water behaves in various PEMs without external humidification and how the self-humidification is obtained or why a high performance can be achieved at PEFCs with the new PEMs in comparison with the conventional PEM.

Experimental Section

Electrolyte Membranes. A recasted Nafion PEM was used in our previous works,[24,25] since the commercialized thin PEM was not available. However, in this work Nafion 112 (50 μm in thickness) was used as a PEM without any additives, denoted as normal-PEM, and as a starting PEM for the preparation of Pt−PEM described below. They were used for the measurements of performances of the cells with these PEMs and for those of non-faradic consumption of reactant gases or production of water, respectively. The reason for the use of Nafion 112 rather than recasted Nafion is to avoid a needless concern about imperfection of the recasted film. Since there was actually no apparent difference in the overall specific resistance or gas permeability between these PEMs, however, they could alternatively be used. Due to the importance of showing the similarity of the recasted PEM, denoted as normal-PEM_R, to the commercialized Nafion 112, some properties of the former will be shown together with those of the latter.

Recasted Nafion PEMs was used for the preparation of PEMs containing TiO_2 or having Pt-probes. The thin PEMs of different thickness (50 or 20 μm) were prepared by casting from Nafion solution (Aldrich).[22] The PEMs of 20 μm thickness were used for the preparation of PEMs with potential probes, the preparation of which will be described below. TiO_2 colloid prepared by the hydrolysis of titanium tetraisopropoxide was used as water-absorbing material. The nanometer-size crystalline TiO_2 [3 weight percent (wt %) to dried Nafion] was added to the Nafion solution, followed by casting to form the oxide-incorporated PEM. This is noted as TiO_2−PEM. A couple of methods for producing a metallic electrocatalytic film near the surface of a PEM have been developed using platinum complexes and reducing agents to form a composite structure used in electrochemical applications.[26,27] In the present work, however, attempting to get a uniform dispersion of Pt nanometer-size crystals inside the PEM, the following procedure was developed.[30] Platinum-complex cations were impregnated in the protonated normal-PEM or TiO_2−PEM by an ion-exchanging reaction with $[Pt(NH_3)_4]Cl_2$ solution containing a projected amount of Pt at 60 °C overnight. They were reduced to Pt nanometer-size crystals with an aqueous solution containing excess neutral hydrazine at room temperature overnight. After washing with pure water, all the PEMs prepared were treated with 3 wt % H_2O_2 solution, then acid-treated with 1 N HNO_3 solution at 60 °C, and finally washed thoroughly with pure water. The resulting PEMs are denoted as Pt−PEM or Pt−TiO_2−PEM, respectively. The amount of Pt in the film, as determined by inductively coupled plasma spectrometry (ICP; SPS1700, Seiko Instrument Inc.), was about 0.09 mg/cm^2. The mean diameter of Pt particles observed by transmission electron microscopy (TEM; JEM-2000FX, JEOL) ranged from 1 to 2 nm, as shown in Figure 2 of ref 25, and that of TiO_2 was ca. 5 nm. Uniform dispersions of Pt and/or oxide particles were observed in whole membrane portions. The PEMs prepared were cut into a sheet 3.5 cm in diameter.

PEMs equipped with potential probes were prepared in the same manner reported in our previous paper.[17] As schematically shown in Figure 1 of ref 17, each piece of three fine Pt wires (25 μm in diameter), which worked as a potential probe (abbreviated by P1, P2, and P3 from anode side to cathode side) for the measurement of ohmic resistance of a different portion in a PEM, was placed with a 120° angle between each two of the four PEM sheets (20 μm in thickness) prepared above. They were hot-pressed at 130 °C for 3 min under 50 kg/cm^2, resulting in 60−65 μm in thickness. Since the thickness was less than the total size of the three probe wires, a projection of each probe apparently overlapped each other partially in the sectional plane of the PEM, although the probes were never in contact directly with each other. As described below, a representative position of each probe was determined by considering that the position corresponded to the center of each probe wire.

Electrode and Cell Operation. The anode and cathode contained 0.37 mg/cm^2 of Pt electrocatalyst of a mean particle diameter of 2.5 nm, respectively. The Pt electrocatalyst, which was supported by 20 wt % on a carbon black of a mean particle diameter of 40 nm, was coated with Nafion thin film in advance and then formed the catalyst layer on a wet-proofed carbon paper (120 μm in thickness) by hot-pressing at 130 °C for 3 min under 50 kg/cm^2. The preparation of these electrodes is described in more detail elsewhere.[17,22] The electrodes attached to each PEM with or without probes, described above, were assembled into a test cell housing of circular shape equipped with a dynamic hydrogen reference electrode, as shown in Figure 2 of ref 28. All cells were operated first with dry H_2 and O_2 at a constant cell temperature $T_{cell} = 80$ °C under ambient pressure, after the cells were dried overnight with dry N_2. But, the Pt−TiO_2−PEM cell was additionally operated with slightly humidified H_2 and O_2, which were saturated with water at $T_H = 35$ °C

($P[H_2O] = 0.056$ atm). In the present work, the flow rates of inlet gases were controlled with mass-flow controllers so as to keep constant utilization of H_2 at 70% and O_2 at 40% for various current densities, which were more practical operation condition than those of previous works[24,25] attempting to demonstrate clearly the superior performances of the new PEMs under extremely dry conditions. To evaluate the mass balance among H_2, O_2, and H_2O under the cell operation, humidities of the exhaust gases from the anode and cathode were measured with electronic humidity sensors (AY-22, Yamato Scientific Instruments). Flow rates of the dried gases in the exhausting gases were measured by thermal conductive mass-flow meters after trapping water with ice traps. The entire of setup of the system is the same as that of the previous work, shown in Figure 2 of ref 30.

Measurements of Cell Performances. Current−voltage (*I*−*V*) curves were measured at the cells using various PEMs without potential probes under steady-state operation with a current interrupter (NCPG 1010, Nikko Keisoku). Overall PEM resistances between the anode and cathode were measured by applying current-off pulses for 100 μs and recording the resulting potential responses with a storage oscilloscope (Hitachi VC 6023). Ohmic potential drops (*iR* drops) in PEMs were included in all current density terminal voltage (*I*−*V*) curves reported here. However, *iR*-free polarization curves for the anodes and cathodes were also shown, potentials of which were referred to a reversible hydrogen electrode (RHE).

Probe Positions and PEM Resistances. The overall resistance and the resistances of various thickness portions from the anode side to cathode side in each PEM were also measured at the cells using PEMs with potential probes under the steady-state current-drawing condition in the same manner as the measurement of *iR* drop described above. To determine the probe distances, the PEMs were uniformly humidified overnight from both sides of the anode and cathode with hydrogen gas saturated with water at 90 °C after the experiments described above, and then the resistances were measured by applying a current-on pulse for 100 μs and recording the resulting potential responses. Assuming that each resistance is proportional to the distance between the corresponding probes, the distance was estimated by multiplying the ratio of the resistance of each portion to the total resistance by the PEM thickness. Thus, the average specific resistance (ρ) between any two probes or the probe and electrode was calculated by dividing each portion's resistance measured above by the corresponding distance.

Results and Discussion

Cell Performances. As shown in Table 1, Pt dispersion in the normal-PEM or TiO_2−PEM did not change noticeably the water absorbability of the PEMs, ΔW, but TiO_2 dispersion in the normal-PEM or Pt−PEM increased them more than 2 times. This clearly shows that TiO_2 played a role to maintain the humidity in the PEMs. On the other hand, Pt dispersion in the normal-PEM and TiO_2−PEM improved the open-circuit voltages (OCVs) noticeably, but TiO_2 dispersion in the normal-PEM or Pt−PEM did not do so. Since the OCV is a good measure of H_2 or O_2 crossover through the PEMs to the cathode or anode, respectively, the result indicates that the dispersed nanometer-size Pt particles mainly contributed to suppress the crossover of the reactant gases. Such contributions of the additives brought about the distinctive improvement of the cell performances under the nonhumidified operation conditions.

TABLE 1: Effect of the Addition of Nanometer-Size Pt and/or Oxide Particles to Normal-PEM on the Water Absorbability or Reactant Crossover Suppression[a]

PEM	ΔW/wt %	OCV/V	$J(H_2)_{th}$/A cm^{-2}
normal-PEM	16.9	0.82	0.177
Pt−PEM	18.2	0.95	0.001
TiO_2−PEM	39.0	0.91	0.006
Pt−TiO_2−PEM	37.9	0.96	0.001>

[a] ΔW, the water absorbability evaluated by measuring the weight change in the predried films after they were equilibrated with water vapor at 60 °C. OCV; the open-circuit voltage as the PEFC with each PEM operated at 80 °C under the flow rate of 2.3 mL/min for the dry reactants of H_2 and O_2. $J(H_2)_{th}$; the calculated amount of H_2, which crossovers into the cathode catalyst layer (see the text and ref 25).

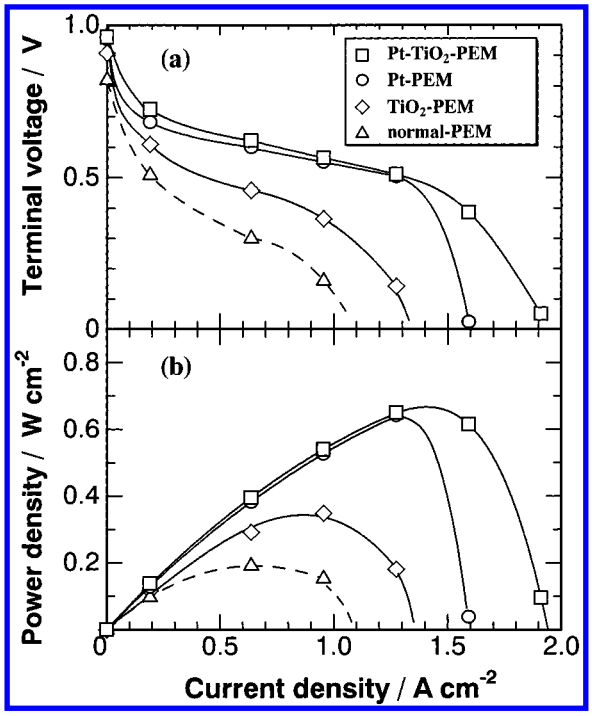

Figure 2. Performances of PEFCs using various PEMs (50 μm in thickness) operated at 80 °C and ambient pressure without any external humidification. Terminal voltage (a) and power density (b) at the reactant utilization: $H_2 = 70\%$, $O_2 = 40\%$.

Figure 2a shows *I*−*V* curves for PEFCs with normal-PEM, TiO_2−PEM, Pt−PEM and Pt−TiO_2−PEM, under nonhumidified condition, and Figure 2b shows the resulting power curves. Although no current could be drawn on the normal-PEM cell at low reactant utilization such as 20% for H_2 and 10% for O_2 due to drying-up of the electrolyte,[24,25] it can work under the present high-utilization conditions described in the Experimental Section. However, it still showed the poor *I*−*V* curve, resulting in the poor output performance, e.g., 0.2 W/cm^2 at 0.6 A/cm^2 and 0.33 V. Compared with this normal-PEM cell, it is found that by using the new PEMs the cell performances are dramatically improved in the cell voltages and the current densities. The order of the improvement is TiO_2−PEM < Pt−PEM < Pt−TiO_2−PEM, as expected from our design concept. The cell voltage gains of ca. 0.2 and 0.4 V were achieved at 0.6 A/cm^2 by using TiO_2−PEM and Pt−PEM or Pt−TiO_2−PEM, respectively, compared with that of normal-PEM. In particular, the combination of Pt and TiO_2 showed superiority in the maximum output, i.e., ca. 0.7 W/cm^2 at 1.6 A/cm^2 and about 0.50 V. The extreme improvement of the performance will be ascribed to a self-humidification at the new PEMs.

Resistances of PEMs. Changes of overall resistances in PEMs without any external humidification are shown in Figure 3 as a function of current density. The resistance of the normal-

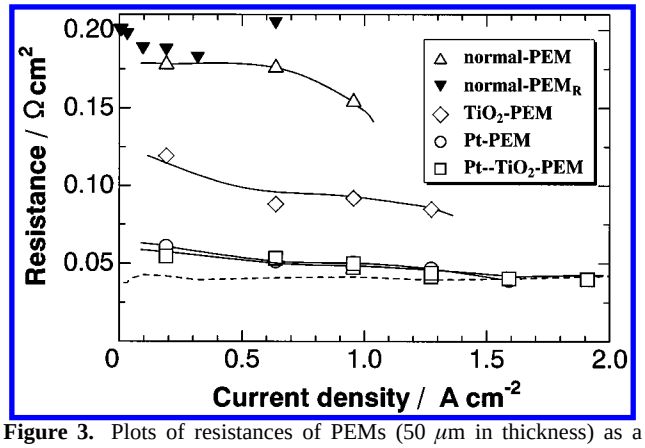

Figure 3. Plots of resistances of PEMs (50 μm in thickness) as a function of current density in PEFCs. The result on a recasted normal-PEM_R (60 μm in thickness) is shown additionally. The operation conditions of the cells are the same as those of Figure 2. The dotted line in the figure represents the resistance of normal-PEM fully humidified at T_H = 90 °C.

PEM (Nafion 112) under the present high reactant utilization decreased by 3 orders of magnitude compared with that under low utilization.[24,25] It is still large, i.e., ca. 0.18 Ω cm^2 at the current density less than 0.6 A/cm^2, and decreases slightly at a higher current density due to the humidification by back-diffused water from the cathode. A recasted normal-PEM_R (60 μm in thickness) also exhibited a resistance level of the normal-PEM. In previous works, an increase of the overall resistance with increase of the drawing current density was shown by numerical predictions[11,12] and also by experiment[19] for thick PEMs such as Nafion 117 in the PEFCs under externally humidifying conditions. It was also shown that the reduction of the overall resistance could be obtained by the decrease of the PEM thichness,[11] e.g., a negligible small increase in the resistance for the PEM of 50 μm thickness, resulting from the back-diffusion of the water produced at the cathode. However, there was no prediction for reduction of the overall resistance at a high current density to a value less than that at a small current density, unlike the present experimental results shown in Figure 3. The experimental result suggests that the back-diffusion of water from the cathode is the major motive force for the water transport in the thin PEM rather than the electroosmotic drag under the present nonhumidified and high current density operating conditions.

The resistance of TiO_2−PEM decreased by half, i.e., ca. 0.09 Ω cm^2, compared with that of normal-PEM. The Pt−PEM or Pt−TiO_2−PEM showed a small resistance of ca. 0.06 Ω cm^2 even at a low current density, resulting from the self-humidification with water produced by the recombination of crossover H_2 and O_2 on the nanometer-size Pt crystals in the PEM, as clarified below. Adding to this effect of Pt and/or TiO_2, the resistance decreased further with an increase in current density due to the back-diffused water, finally to the value of 0.04 Ω cm^2 (or 8 Ω cm) at around 1.6 A/cm^2. This value coincides with that of the normal-PEMs fully humidified by supplying H_2 gas saturated with water vapor at T_H = 90 °C (shown by the dotted line). However, this overall reduction in the electrolyte resistance corresponds to the *iR* drop of ca. 0.06 V at 0.6 A/cm^2, so that cannot explain fully such a large cell voltage gain of 0.4 V, as described in the above section for the *I*−*V* curves at PEFCs with Pt−PEM or Pt−TiO_2−PEM. Therefore, it is essential to see the humidification behavior in more detail.

Distribution of the Specific Resistances in PEMs. Figure 4 shows the relationship between the average specific resistance,

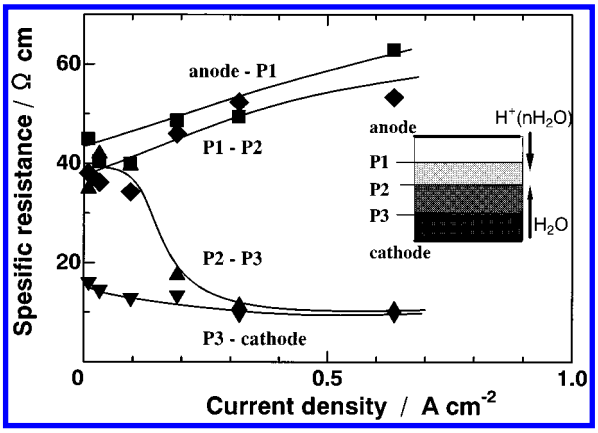

Figure 4. Specific resistances of different portions in normal-PEM (60 μm in thickness, with potential probes) as a function of current density. The operation conditions of the cells are the same as those of Figure 2.

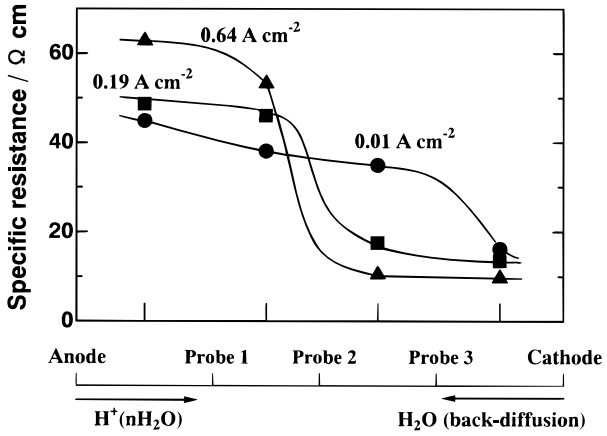

Figure 5. Specific resistances at various current densities in normal-PEM (60 μm in thickness, with potential probes) as a function of potential-monitoring probe position. The operation conditions of the cells are the same as those of Figure 2.

ρ, and the current density at different portions in the normal-PEM operating with dried reactant gases at 80 °C. The ρ values from the anode to P1 and from P1 to P2 increase with the increase of current density, but those of the cathode side decrease. This trend well represents the electroosmotic drag behavior, which has been discussed theoretically in PEMs.[11] Then, the ρ values are replotted as a function of probe positions in Figure 5. The fractional position of each probe, indicated in the *x*-axis between the anode and cathode, and the ρ value were determined as described in the Experimental Section. Therefore, one can know the practical resistance of each portion by multiplying the distance by the corresponding average specific resistance. Total resistances of each portion agreed well with a resistance measured singly between the anode and cathode within experimental error accompanying reading storage data on the oscilloscope at the *iR* drop measurement, i.e., less than several percent, for all experimental sets. At a small current density of 0.01 A/cm^2, the ρ distribution is relatively flat overall the positions, except the ρ from P3 to the cathode. However, it is clearly shown that the ρ values of the anode side increase with increasing current density, but those of the cathode side decrease extremely, resulting in the appearance of a critical boundary of the ρ distribution at the middle part of the membrane depth. A similar tendency was observed on the normal-PEM_R (50 μm thickness) in our previous work under humidification for the anode alone at various temperatures (T_H), as the cell temperature (T_{cell} = 80 °C) was lower than the T_H.[17]

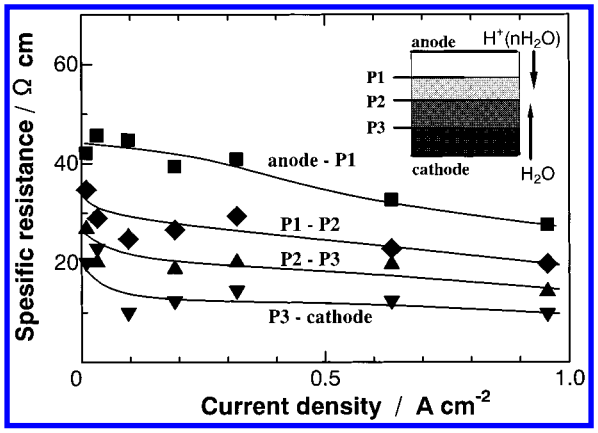

Figure 6. Specific resistances of different portions in Pt−PEM (60 μm in thickness, with potential probes) as a function of current density. The operation conditions of the cells are the same as those of Figure 2.

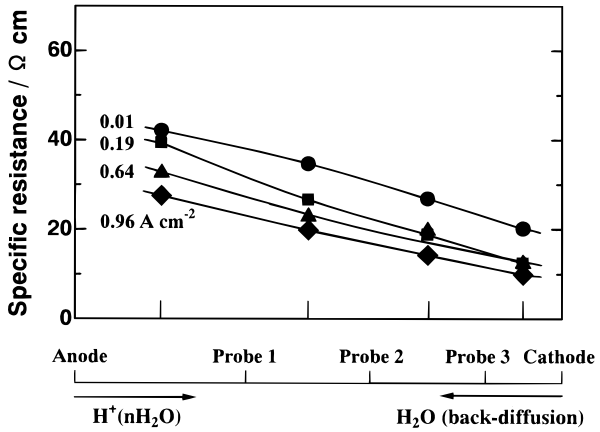

Figure 7. Specific resistances at various current densities in Pt−PEM (60 μm in thickness, with potential probes) as a function of potential-monitoring probe position. The operation conditions of the cells are the same as those of Figure 2.

When the T_H was elevated, e.g., to $T_H = 90$ °C, the ρ values at the anode side declined substantially, but did not reach to the minimum value. The mathematical modeling and numerical calculation showed a large change of water content (H_2O/SO_3^-) in Nafion 117 between the anode and cathode as the current density increased;[11,12] for example, the content ratios at the anode and cathode were 13/14 for 0.1 A/cm^2 and 3/15 for 0.8 A/cm^2, respectively, at $T_{cell} = T_H = 80$ °C.[11] However, the calculated distributions in the PEM were relatively monotonic,[11,12] because of the estimation for the sufficiently humidified anode and cathode that was different from our experimental conditions. As will be shown in a later section, it was found that performances of the anode and cathode are strongly dependent on the ρ distribution, but not as much on the overall resistance in the PEM. The numerical analyses are generally very important due to the flexibility of the application to experimentally difficult conditions or materials, but such simulation results have to be substantiated by the in situ experimental evidence. The use of our experimental method may be extended to many experimental conditions or any thicker PEMs.

As shown in Figure 6, it is found at the Pt−PEM that the ρ values of all portions decrease with increasing current density, which are extremely distinctive from those of the normal-PEM shown in Figure 4. The ρ decreases monotonically from the anode side to the cathode side and decreases with increasing current density, as shown in the replotted Figure 7. A linear relationship between the conductivity and water content in Nafion 117 was shown.[29] Thereby, it is considered that a uniform distribution of the specific resistances shown in Figure 7 may reflect a uniform distribution of water in the Pt−PEM under various current densities. Such a water distribution may be brought by the complement to the water transferred by electroosmotic drag with that formed inside the PEM by the recombination of crossover gases and that back-diffused from the cathode. The mechanism will be clarified below.

The uniformity of the ρ distribution profile can be further improved at the Pt−TiO_2−PEM, as shown by dotted lines in Figure 8. As clear in the comparison with the data on Pt−PEM shown in Figure 7, the reduction of the specific resistances of the anode side is larger than that of the cathode side by the cooperation of hygroscopic TiO_2 with the Pt−PEM, resulting in a more uniform ρ distribution over the entire portions of the Pt−TiO_2−PEM. The achieved ρ value is ca. 20 Ω cm at a high current density region (> ca. 0.5 A/cm^2). The homogenizing effect by TiO_2 on the ρ distribution is emphasized more as

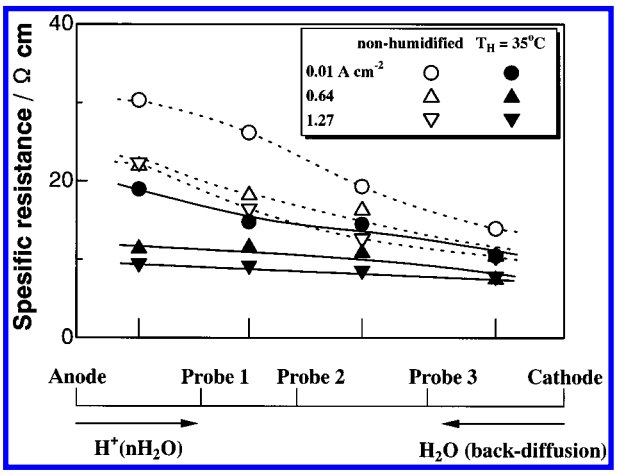

Figure 8. Specific resistances at various current densities in Pt−TiO_2−PEM (65 μm in thickness, with potential probes) as a function of potential-monitoring probe position. The PEFCs were operated at 80 °C and ambient pressure, without any external humidification (dotted lines) or slightly humidified at 35 °C (solid lines; $P[H_2O] = 0.056$ atm). Reactant utilization: $H_2 = 70\%$, $O_2 = 40\%$.

the reactant gases are slightly humidified with water vapor of 0.056 atm (saturated at 35 °C), as shown by solid lines. The minimum ρ value of 10 Ω cm can be achieved overall the PEM portions at a practically operational current density.

Thus, a great difference has been found in the ρ distribution between the normal-PEM and the proposed new PEMs, which could not be predicted just by the measurement of the overall resistances. The uniform and small resistance in Pt−TiO_2−PEM makes the PEFC operation without any serious performance loss possible under either completely dried or slightly humidified reactant gases.

Amounts of Non-Faradic Consumption of H_2 and O_2. Figure 9 shows the total amounts of H_2 and O_2 consumed in the cells with different PEMs as a function of output current densities. The consumption of each gas is larger than that calculated from Faraday's law (shown by a solid line) for each anode and cathode reaction. The ratio of H_2 to O_2 remains in the stoichiometric ratio of 2 for all experimental sets, independent of the amounts of their consumption. As described in the next section, the sum of the water amounts exhausted from both compartments of anode and cathode was also larger than that calculated from Faraday's law. The water thus excessively produced in each cell with different PEM was found to coincide well with that of the water calculated by assuming the formation

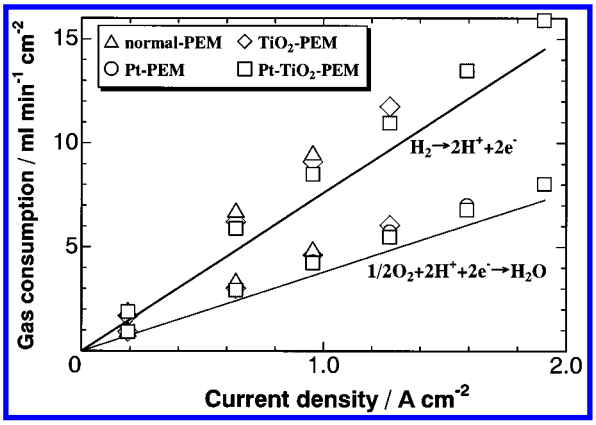

Figure 9. Overall consumption of H_2 and O_2 in the PEFCs with various PEMs (50 μm in thickness) as a function of current density. The operation conditions of the cells are the same as those of Figure 2. The solid lines represent the relationships between the faradic consumption of H_2 and O_2 and the current density.

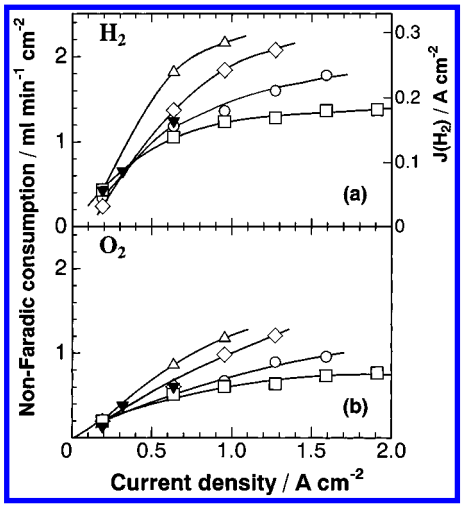

Figure 10. Non-faradic consumption of H_2 (a) and O_2 (b) in the PEFCs with various PEMs (50 μm in thickness) as a function of current density estimated on the basis of the results shown in Figure 9. As a reference, the result on a recasted normal-PEM_R (60 μm in thickness) is also shown with (▼) symbols.

from the excessively consumed H_2 and O_2, as shown in Figure 11. This clearly indicates that the excess water is generated by a non-faradic reaction relating to the crossover H_2 and O_2 but not by the electrochemical cell reaction. Then, the amounts of H_2 and O_2 consumed by the non-faradic process in the normal-PEM or Pt and/or TiO_2 dispersed PEMs were estimated by subtracting the amounts of consumption calculated by Faraday's law from those of the total consumption measured.

The results are shown in Figure 10a with the equivalent current density $J(H_2)$ (right axis) based on the H_2 consumption as a function of the current density drawn from the cells under constant utilization of H_2 and O_2. The results for the O_2 consumption are also shown in Figure 10b. Accuracy of all the data is justified by their good regression measured independently into a linear line of the ratio of $H_2/O_2 = 2$, as seen in the inset of Figure 11. In every cell, the non-faradic consumption resulting from the crossover clearly increases with increasing current density. Amounts of the consumption at high current density, particularly at the normal-PEM using Nafion 112, seemed to be too large by intuition, although the consumption at zero-current density was sufficiently small, i.e., nearly zero. As shown in the same figure, a recasted normal-PEM_R exhibits behavior similar to that of the normal-PEM, although

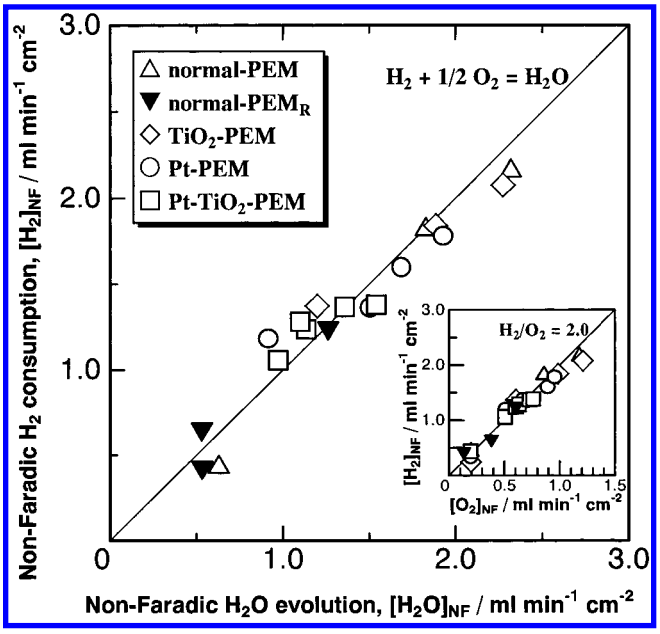

Figure 11. Relationship between the total amounts of excessively consumed H_2, $[H_2]_{NF}$, and those of H_2O excessively produced, $[H_2O]_{NF}$, via non-faradic reactions, respectively, which are evaluated on the basis of the independent experiments. The solid line shows the consumed amounts of H_2 predicted from the amounts of H_2O experimentally measured. The inset shows the relationship between the $[H_2]_{NF}$ and $[O_2]_{NF}$, which are the amounts of H_2 and O_2 excessively consumed via non-faradic electrode reactions, respectively. The solid line shows the ratio of $H_2/O_2 = 2$. The results on a recasted normal-PEM_R (60 μm in thickness) are also shown as a reference.

the amount of crossover is a little suppressed compared with the latter probably due to the 20% larger thickness. We have not seen any published crossover data that are measured in a cell operated with completely dried gases such as ours, but many papers have studied the permeability of H_2 and/or O_2 in commercialized Nafion membranes or recasted ones in solutions such as diluted acids.[31−39] Let's first estimate the amounts of crossover in the normal-PEM contacting with liquid water. All the reported products of diffusion coefficient and concentration of dissolved gas in PEM, D_fC_f, are within an order of magnitude difference for both PEMs types. Using a D_fC_f value of 10.7 mM cm^2 s^{-1} for H_2 at 60 °C,[39] the estimated amount of crossover in the PEM of 50 μm thickness becomes 0.83 mA cm^{-2}, which is 2 orders of magnitude smaller than the $J(H_2)$ observed in the present work. Therefore, we have carefully checked possibilities of any experimental faults such as some problems with material balance measurements or with gas leakage around PEMs or via a tear of PEMs. As seen in the inset of Figure 11, the accuracy and reproducibility of all data on the amounts of H_2 and O_2 consumed are justified with their very small deviation from the stoichiometric reacting ratio at the cells with any PEMs used. They are confirmed further by the good stoichiometric coincidence of the excessively produced H_2O with the excessively consumed H_2, which are measured independently (see Figure 11). The data shown in Figure 9, as well as those in Figure 10, were obtained under setting of flow rates of H_2 and O_2 manually at each current density so as to keep the utilization constant, resulting in some unavoidable scattering of the pressure difference between the anode and cathode. If there is any gas leakage around PEMs or via a tear of PEMs, a large scattering of the data of the non-faradic gas consumption must appear in Figure 11. Nevertheless, there is no evidence of it.

On the other hand, a recasted normal-PEM_R exhibited no noticeable difference from the normal-PEM (Nafion112) in the behaviors of the consumption of reactant gases or production of water, as shown in Figures 10 and 11 and later in Figure 12. This normal-PEM_R showed a very low OCV of ca. 0.85 V under the dry-gas operation (see Table 1 of ref 25) approximately the same as the 0.82 V for the normal-PEM in the present work, but under a sufficiently humidified condition it showed not only a very high OCV but also the same superior current−voltage property as those of Pt−PEM or Pt−oxide−PEMs (refer to Figure 5 of ref 25). This is more evidence that the low OCV of the normal-PEM_R or the normal-PEM in the present work is not a result of any direct gas leakage around PEMs or via a tear of PEMs but of the intrinsic gas permeability of the PEMs. It is also important to emphasize that the consumption of reactant gases at zero-current density is sufficiently small, i.e., nearly zero or "no direct leakage" in all types of PEMs examined even under the present dry conditions. Of course, we have confirmed carefully the reproducibility of the data shown here on the normal-PEMs by using different experimental sets. Thus, we conclude that the unusual high rates of crossover in the present work do not appear to be due to any experimental or calculating faults but to the difference of the experimental conditions from those in previous works for the measurements on crossovers[31−39] or cell performances, i.e., the cell operation with dry gases under drawing of a large current in the present work.

The remaining important issue is how we are able to explain the large dependence of the non-faradic consumption on the drawing current density, particularly at the high current density region. The increase of the consumption with increasing current density must be ascribed to a reduction of mass-transport barrier in gas diffusion layers crossing to the electrode−electrolyte interfaces with increased flow rates of dry reactant gases so as to keep the reactant utilization constant. The effect will be discussed further in the Polarization Properties section.

The consumption slows down at a high current density probably because of the increased humidification of PEMs mainly by the back-diffused water from the cathode. But, $J(H_2) = 0.28$ A/cm^2, namely, more than 20% of the total H_2 consumption is still lost at the normal-PEM by the useless recombination reaction at the current drawing of 1.0 A/cm^2. It is evident that the crossover is greatly suppressed at Pt and/or TiO_2−PEMs, in the order of TiO_2−PEM, Pt−PEM, and Pt−TiO_2−PEM. The loss at 1.0 A/cm^2 can be reduced up to two-thirds and a half of that of normal-PEM for the Pt−PEM and Pt−TiO_2−PEM, respectively. This is probably brought by the increased and uniform humidity throughout the new PEMs with the water produced on Pt nanometer-size particles via the recombination reaction of crossover gases. Suppression of the non-faradic consumption of reactant gases at these PEMs extends more as the current density increases in comparison with the normal-PEM, probably due to the increased back-diffusion of the water produced at the cathode as shown later with Figure 12. If there is no restriction to the expansion of PEMs, they can swell freely with increasing water content, e.g., ca. 120% expansion in one direction. At practical installations, however, all PEMs were tightly fixed with attached plates such as current collectors or electrodes consisting of carbon paper in the cell housing under the dry state. As a result, the PEMs could not be freely swelled but rather were compressed by the increased humidification. Thus, it was considered that the crossover of reactant gases via the compressed Pt−PEM and Pt−TiO_2−PEM is extremely suppressed.

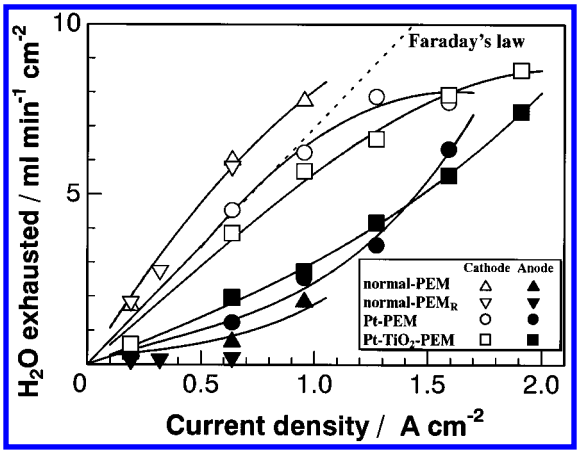

Figure 12. Amounts of water exhausted from the cathode (open symbols) and anode (filled symbols) in PEFCs with various PEMs (50 μm in thickness) as a function of current density. The operation conditions of the cells are the same as those of the Figure 2. The dotted line represents the relationship between the faradic generation of water and the current density. As a reference, the result on a recasted normal-PEM_R (60 μm in thickness) is also shown.

It is important to notice that the consumed H_2 at the Pt−PEM and Pt−TiO_2−PEM is much efficiently used for the PEM humidification differing from that of normal-PEM, as explained in the following sections.

Amounts of H_2O Exhausted into the Anode and Cathode. To clarify where the crossover gases recombine and how the Pt−PEM is self-humidified, the amount of water vapor produced by the recombination and the faradic reaction was analyzed under various operating conditions. Figure 12 shows the amounts of H_2O exhausted from the cathode and anode compartments. The total amounts of H_2O exhausted from both anode and cathode compartments were larger than those calculated on the basis of Faraday's law in the cells with all types of PEMs. The excess water was found to correspond to the amount of water produced from the excessively consumed H_2 and O_2, as in Figure 11 and described in the above section.

In the normal-PEM cell, it was found that the amount of water exhausted from the cathode, $[H_2O]_C$, is larger than that produced by the faradic cathodic reaction, $[H_2O]_F$, shown by a dotted line. The amount of water from the anode, $[H_2O]_A$, is approximately the same or more compared with the cathode excess water. This indicates that the crossover H_2 and O_2 reach the cathode and anode catalyst layers, respectively, and cause the so-called "chemical short-circuit reaction" with O_2 and H_2 supplied to those catalyst layers as reactant gases. This reaction consumes the stoichiometric amounts of reactant gases to the crossover gases. The water thus produced by the reaction is directly exhausted into outlet gas flows via each anode and cathode catalyst layer. Such water may not be used efficiently for the PEM humidification. Similar behavior is also observed at the recasted normal-PEM_R as shown also in Figure 12.

On the other hand, it is particularly important to point out that, in the Pt−PEM cell, the $[H_2O]_C$ equal to the $[H_2O]_F$ is exhausted at a current density less than 0.8 A/cm^2 and the $[H_2O]_C$ less than the $[H_2O]_F$ is exhausted at the current density beyond 0.8 A/cm^2. Contrary, the $[H_2O]_A$ increases with increasing the current density and does so more steeply in the higher current density region. This observation in the low current density region clearly indicates that all of crossover gases recombine inside the Pt−PEM, undoubtedly on dispersed Pt nanometer-size particles, and the formed water diffuses out toward the anode direction. As a result of the complete

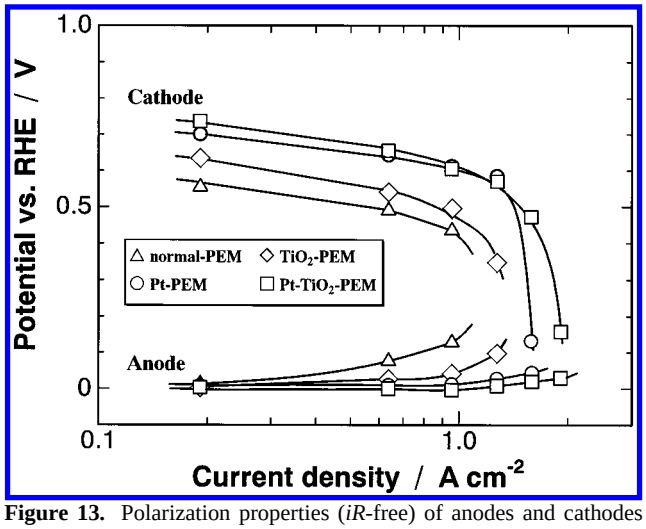

Figure 13. Polarization properties (*iR*-free) of anodes and cathodes in the PEFCs with various PEMs (50 μm in thickness). The operation conditions of the cells are the same as those of Figure 2.

recombination reaction inside the Pt−PEM, the non-faradic H_2 consumption is expected to be less than that in the catalyst layers of the normal-PEM cell, which should be two-thirds providing that the diffusion parameters for H_2 and O_2 in the Pt−PEM are at a level similar to those in the normal-PEM.[39] The expected reduction of the non-faradic loss at the Pt−PEM is consistent with that observed experimentally in Figure 10. The decrease in the $[H_2O]_C$ to less than the $[H_2O]_F$ and the steep increase in the $[H_2O]_A$ in the higher current density region indicate that the water formed by the faradic reaction at the cathode is also back-diffusing to the anode direction in that current density region. All of the water produced inside the Pt−PEM as well as some part of that back-diffused from the cathode may humidify the PEM efficiently, which brings the fairly uniform distribution of the ρ values as we saw in Figure 7.

In the Pt−TiO_2−PEM cell, the $[H_2O]_C$ does decrease to a level less than the $[H_2O]_F$ even at a low current density region and the $[H_2O]_A$ increases more than that of the Pt−PEM cell, resulting in the $[H_2O]_C$ close to the $[H_2O]_A$. In this PEM, TiO_2 does enhance the back-diffusion of the water generated by the faradic reaction at the cathode, with the hygroscopic property. Such a nice water balance between the anode and cathode as seen in Figure 12 over the entire current density region has realized the uniform humidification over the entire portions of Pt−TiO_2−PEM, which is well consistent with the ρ distributions in Figure 8.

Thus, it has been clarified where the crossover gases recombine, why the non-faradic consumption is suppressed, and how the produced water is exhausted in the proposed new PEMs in comparison with those in the normal-PEM.

Polarization Properties. Figure 13 shows the *iR*-free polarization curves at anodes and cathodes of PEFCs with various PEMs. Despite *iR*-free performance for the very fast H_2 oxidation reaction on the Pt catalyst, the anodic polarization in the normal-PEM cell increases steeply with increasing current density, i.e., ca. 0.1 V at 1 A/cm^2. This is because of the lowered proton conductance in the PEM close to the catalyst layer as shown in the above sections and probably in the anode catalyst layer due to the evaporation of water in the dry H_2 stream. However, it is evident that the improved proton conductance at the anode side in Pt−PEM and Pt−TiO_2−PEM, shown by Figures 7 and 8, brings the extreme reduction of the anode polarization.

The advantage of the recombination of crossover gases inside PEMs appears dramatically in the cathode polarization property. The Pt−PEM and Pt−TiO_2−PEM cells exhibit nearly 0.2 V less polarization than the normal-PEM cell. All performances of these cells may be controlled by an electrochemical charge-transfer step, because these polarization curves show the same Tafel slope of ca. −70 mV/decade. Accordingly, the reduction of the cathodic overpotential of 0.2 V at the Pt−PEM or Pt−TiO_2−PEM cells from that of the normal-PEM is ascribed to the improvement of the "effective or real Pt utilization", and the utilization is estimated to be 1000 times larger than that of normal-PEM. We considered first that a reason for this difference could be such varying degrees of cathode catalyst layer hydration by drying as shown in previous work by Uribe et al.[40] However, it could not be adopted as a major factor for the explanation because the cathode hydration levels for the normal-PEM and the others were all at the same level, as clearly shown in Figure 5 and Figures 7 and 8, i.e., $\rho = 10-20\ \Omega$ cm. Let's try to consider another reason for the improvement of the performances at Pt and/or TiO_2 cooperating PEM cells from that at the normal-PEM cell. Since every anode drawing no current exhibited no polarization, each OCV value shown in Table 1 was equal to the *iR*-free cathode potential of each cell. This cathode potential was regarded as a mixed potential, E_{mix}, determined by the balance of the current density for O_2 reduction, $J(O_2)$, and that for crossover H_2 oxidation, $J(H_2)_{th}$, at the cathode. The $J(H_2)_{th}$ was given by the following equation similar to our previous work[25] and to the conventional relationship for metal corrosions.

$$\log J(H_2)_{th} = \log J(O_2) = -n\alpha_c F[E_{mix} - E(O_2)]/2.303RT + \log J_0(O_2) \quad (1)$$

Here, $E(O_2)$ and $J_0(O_2)$ are the reversible potential and the exchange current density for O_2 reduction under the operating conditions, respectively, and $n\alpha_c$ and F have their usual meanings. The values of $J_0(O_2)$ and $n\alpha_c$ were determined on the basis of the Tafel plots shown in Figure 13. The value of $E(O_2)$ was calculated by using the free energy for the cell reaction at 80 °C, $\Delta G° = -26.0$ kJ/mol, a partial pressure of water vapor at 50 °C, $P[H_2O] = 0.122$ atm, and the balance of the partial pressure for oxygen, $P[O_2] = 0.878$ atm. Values of $J(H_2)_{Th}$ in Table 1 show the amounts of crossover H_2 via normal-PEM, Pt−PEM, TiO_2−PEM, and Pt−TiO_2−PEM, estimated by applying these values to eq 1. (We assumed that the cathode catalyst layer was in equilibrium with the water vapor saturated at 50 °C, since it was very difficult to estimate the actual vapor pressure. The assumption did not make much difference in the estimated $J(H_2)_{th}$ compared with that for the cell temperature of 80 °C.) On the other hand, the experimental values of $J(H_2)$ at zero current density were approximately zero for all PEMs including the normal-PEM as seen in Figure 10. The results are well consistent with the $J(H_2)_{th}$ for the Pt−PEM, TiO_2−PEM, and Pt−TiO_2−PEM. However, the $J(H_2)_{th}$ value for the normal-PEM deviates exceptionally from the experimental data. This large value, misled from eq 1, may result from the use of the $E(O_2)$ value larger than the actual one and accordingly that of the $J_0(O_2)$ value smaller than the actual one. In other words, the actual $P[O_2]$ for the estimation should be negligibly small in the cathode catalyst layer of the normal-PEM cell. ($P[H_2O]$ may be larger than that saturated at 80 °C due to the supersaturation or the local heating brought by the exothermic cathode reaction, but it is not more than an ambient pressure.) This consideration can strongly be supported by the fact described in the above section; that is, at the normal-PEM cell, all crossover H_2 reacts in the cathode catalyst layer by the

chemical short-circuit reaction, and the resulting water flux leaving the cathode makes O_2 diffusion to the inner layer extremely difficult. Thus, it is considered that most of the Pt electrocatalyst particles in the cathode may be useless, that is, in the abnormal level of 1/1000 compared to the Pt utilization at the new Pt−PEM and Pt−TiO_2−PEM.

On the contrary, at Pt−PEM and Pt−TiO_2−PEM cells, all the water produced by the recombination of crossover H_2 and O_2 in the PEMs is exhausted toward the anode side, resulting in no restriction of O_2 diffusion to the inner catalyst layer. As a result, the improved Pt catalyst utilization and such less polarization as ca. 0.2 V compared with that of the normal-PEM cell must be achieved at the cathode.

Conclusion

Thus, we clarified how the self-humidification behavior is different among the normal-PEM and the Pt and/or oxide-PEMs under externally nonhumidified conditions and the mechanism why such a very high performance can be achieved at the PEFCs with the new PEMs. As described in the Discussion section, the uniform ρ distribution reflecting the water distribution in PEMs is extremely important in the achievement of high-performance PEFCs. Performances of the cells with Pt−PEM or Pt−TiO_2−PEM could be improved at 1 A/cm^2 by 0.1 V at the anode and 0.2 V at the cathode resulting from homogenizing the ρ distribution, and additionally by 0.1 V at the ohmic loss resulting from reducing the overall resistance of the PEM, compared with those of normal-PEM. The new PEMs operating with no or minimal humidification are particularly important for the PEFCs applied to the power sources of electric vehicles or various electronic devices from the viewpoints of the simplification of control systems, cold starts, or response to abrupt load changes, when the PEFCs will be operated with dry H_2 and/or dry air, particularly under an ambient pressure.

Acknowledgment. This work was partially supported by the funds of the Research Institute of Innovative Technology for the Earth (RITE) and by the Grant-in-Aid No. 09237104 for Scientific Research on Priority Area of “Electrochemistry of Ordered Interfaces”.

References and Notes

(1) Yeo, R. S. *J. Electrochem. Soc.* **1983**, *130*, 533.
(2) Pushpa, K. K.; Nandan, D.; Iyer, R. M. *J. Chem. Soc., Faraday Trans.* **1988**, *84*, 2047.
(3) Ticianelli, E. A.; Derouin, C. R.; Redondo, A.; Srinivasan, S. *J. Electrochem. Soc.* **1988,** *135*, 2209.
(4) Verbrugge, M. W.; Hill, R. F. *J. Electrochem. Soc.* **1990,** *137*, 886.
(5) Bernardi, D. M. *J. Electrochem. Soc.* **1990**, *137*, 3344.
(6) Zawodzinski, T. A., Jr.; Springer, T. E.; Davey, J.; Jestel, R.; Lopez, C.; Valerio, J.; Gottesferd, S. *J. Electrochem. Soc.* **1993,** *140*, 1981.
(7) Zawodzinski, T. A., Jr.; Derouin, C.; Radzinski, S.; Sherman, R. J.; Smith, V. T.; Springer, T. E.; Gottesfeld, S. *J. Electrochem. Soc.* **1993**, *140*, 1041.
(8) Zawodzinski, T. A., Jr.; Neeman, M., Jr.; Sillerud, L. O.; Gottesferd, S. *J. Phys. Chem.* **1991**, *95*, 6040.
(9) Hinatsu, J. T.; Mizuhata, M.; Takenaka, H. *J. Electrochem. Soc.* **1994**, *141*, 1493.
(10) Staiti, P.; Poltarzewski, Z.; Alderucci, V.; Maggio, G.; Giordano, N.; Fasulo, A. *J. Appl. Electrochem.* **1992**, *22*, 663.
(11) Springer, T. E.; Zawodzinski, T. A., Jr.; Gottesfeld, S. *Proceeding of the Symposium Modeling of Batteries and Fuel Cells*; The Electrochemical Society: Pennington, N. J., 1991; Vol. 91−10, p 209; *J. Electrochem. Soc.* **1991**, *138*, 2334.
(12) Fuller, T. F.; Newman, J. *J. Electrochem. Soc.* **1992**, *139*, 1332; **1993**, *140*, 1218.
(13) Bernardi, D. M.; Verbrugge, M. W. *J. Electrochem. Soc.* **1992**, *139*, 2477.
(14) Tyson, Y.-M.; Kimble, M. C.; White, R. E. *J. Electrochem. Soc.* **1992**, *139*, 1913.
(15) Nguyen, T. V.; White, R. E. *J. Electrochem. Soc.* **1993**, *140*, 2178.
(16) Chen, R. S.; Jayakody, J. P.; Greenbaum, S. G.; Pak, Y. S.; Xu, G.; Maclin, M. G.; Fontanella, J. J. *J. Electrochem. Soc.* **1993**, *140*, 889.
(17) Watanabe, M.; Igarashi, H.; Uchida, H.; Hirasawa, F. *J. Electroanal. Chem.* **1995,** *399*, 239.
(18) Hlim, J.; Büchi, F. N.; Haas, O.; Stamm, M.; Scherer, G. G. *Electrochim. Acta* **1994**, *39*, 1303.
(19) Büchi, F. N.; Scherer, G. G. *J. Electroanal. Chem.* **1996**, *404*, 37.
(20) Xie, G.; Okada, T. *J. Electrochem. Soc.* **1995**, *142*, 3058.
(21) Bellows, R. J.; Lin, M. Y.; Arif, A.; Jacobson, D. *The 1997 Joint International Meeting Abstracts;* The Electrochemical Society and International Society of Electrochemistry: Paris, 1997; Vol. 97−2, p 1102.
(22) Watanabe, M.; Sakairi, K.; Inoue, M. *J. Electroanal. Chem.* **1994,** *375*, 415.
(23) Watanabe, M. U.S. Patent, 05472799, 1995.
(24) Watanabe, M.; Uchida, H.; Seki, Y.; Emori, M. *The 186th Meeting Extended Abstracts;* The Electrochemical Society: Miami, FL, 1994; Vol. 94−2, p 946.
(25) Watanabe, M.; Uchida, H.; Seki, Y.; Emori, M.; Stonehart, P. *J. Electrochem. Soc.* **1996**, *143*, 3847.
(26) Takenaka, H.; Torikai, E. Kokai Tokyo Koho (Japan Patent), 55, 38934, 1980.
(27) Liu, R.; Her, W.-H.; Fedkiw, P. S. *J. Electrochem. Soc.* **1993**, *139*, 15.
(28) Watanabe, M.; Satoh, Y.; Shimura, C. *J. Electrochem. Soc.* **1993**, *140*, 3191.
(29) Zawodzinski, T. A., Jr.; Springer, T. E.; Davey, J.; Valerio, J.; Gottesfeld, S. *Proceeding of the Symposium Modeling of Batteries and Fuel Cells*; The Electrochemical Society: Pennington, NJ, 1991; Vol. 91−10, p 187.
(30) Watanabe, M.; Uchida, H.; Emori, M. *J. Electrochem. Soc.* **1998,** *145*, 1137.
(31) Ogumi, Z.; Kuroe, T.; Takehara Z. *J. Electrochem. Soc.* **1985**, *132*, 2601.
(32) Fritts, S. D.; Gervasio D.; Zeller, R. Z., III; Savinell, R. F. *J. Electrochem. Soc.* **1991**, *138*, 3345.
(33) Ogumi, Z.; Kuroe, T.; Takehara, Z. *J. Electrochem. Soc.* **1984**, *131*, 769.
(34) Wakizoe, M.; Kim, J.; Srinivasan, S.; MacBeen, J. *Proceedings of the Symposium on Batteries and Fuel Cells for Stationary and Electric Vehicle Applications*; The Electrochemical Society: Pennington, NJ, 1993; Vol. 93−8, p 310.
(35) Sakai, T.; Takenaka, H.; Yoshizawa, S. *J. Electrochem. Soc.* **1986**, *133*, 88.
(36) Gottesfeld, S.; Raistrick, I. D.; Srinivasan, S. *J. Electrochem. Soc.* **1987**, *134*, 1455.
(37) Lawson, D. R.; White, L. D.; Martin, C. R.; Szentirmay, M. N.; Song, J. I. *J. Electrochem. Soc.* **1988**, *135*, 2247.
(38) Parthasarathy, A.; Martin C. R.; Srinivasan, S. *J. Electrochem. Soc.* **1991**, *138*, 916.
(39) Watanabe, M.; Igarashi, H.; Yoshioka, K. *Electrochim. Acta* **1995**, *40*, 329.
(40) Uribe, F. A.; Springer, T. E.; Gottesfeld, S. *J. Electrochem. Soc.* **1992**, *139*, 765.